Applications of quantitative T1, T2, and proton density to diagnosis

Kevin J. Chang, MD and Hernán Jara, PhD

Quantitative magnetic resonance imaging (Q-MRI) differs sharply from conventional directly acquired MRI in that objective measures (such as the trio of basic MR properties: T1, T2, and proton density(PD)) are used for analysis as well as further postprocessing rather than relative signal intensities. This paper will recount a brief history of the origins and applications of Q-MRI for measurement of T1 and T2 relaxation times and PD, as well as discuss the basic theoretical underpinnings. A variety of postprocessing options as well as a review of the scientific literature regarding clinical applications of these techniques over the past 30 years are addressed.

Most radiologic interpretation with magnetic resonance (MR) imaging has focused on qualitative visual assessment of anatomy and disease processes rather than quantitative analysis. This method of interpretation has served to define gross extent of disease when anatomic changes manifest as visibly detectable differences in signal intensity. If scan parameters and timings are not set optimally prior to scanning or if the patient is unable to cooperate throughout the entire length of a study, qualitative interpretation of the resulting directly acquired images suffers dramatically. In these ways, the current conventional practice of MR imaging may be seen as relatively inefficient in the extraction of MR information from tissues and organs when compared with quantitative MR imaging (Q-MRI) techniques.

Conventional or directly acquired MR images are qualitative and contrast-weighted where pixel values have meaning only in relation to other pixel values. These pixel values are dependent on a complex mix of proton density (PD), longitudinal relaxation time (T1), and transverse relaxation time (T2) based on the initial scan settings. Q-MRI portrays the spatial distribution of absolute biophysical parameter measurements on a pixel-by-pixel basis. Biophysical parameters quantified by Q-MRI include the primary triad of T1, T2, and PD. Other parameters currently measured in clinical practice are the diffusion coefficient and diffusion tensor, perfusion, and blood-oxygen–level dependence (BOLD) in functional MR imaging. Quantitative parameters investigated experimentally have also included T2*, T1ρ, and the magnetization transfer ratio. These quantitative measures are theoretically independent of experimental settings (such as magnetic and radiofrequency [RF] field, inhomogeneity, receiver gain, and coil sensitivity), and are thus absolute and comparable between different scanners, different institutions, and over differing points in time.

Quantitative and qualitative MR imaging offer complementary medical information and use the same technology platform and equipment. While the patient information generated with conventional scanning is primarily visual, Q-MRI portrays information that is intrinsically more tissue-specific and is consequently less dependent on subjective visual assessment. The quantitative data generated by Q-MRI (eg, T1, T2, and PD maps) can also be postprocessed to take advantage of new ways of looking at the wealth of information available such as segmentation based on biophysical properties and anatomy, distribution histograms, and synthetic MR images of user-definable and variable weighting (variable at the time of image interpretation).

The purpose of this paper is to delineate the principles of Q-MRI relaxometry and to provide a review of its clinical applications.

Quantitative MR imaging principles

Differential weighting

The defining aspect of quantitative image information, as opposed to qualitative image information, is that quantitative pixel values are devoid of extraneous experimental information and are therefore largely tissue-specific. Accordingly, Q-MRI may be viewed as a collection of MR imaging techniques with which the tissue-specific information contained in the directly acquired images can be separated from experimental conditions.

Generating quantitative MR images of the human body is accomplished in 2 phases. First, a Q-MRI pulse sequence is employed to generate directly acquired images. For every slice, there are 2 or more images that are identical in all experimental conditions except for the weighting in the target parameter (eg, T1, T2, etc). In the second phase, these differentially weighted images are processed with a Q-MRI algorithm used for computing maps of the target parameter. The focus of this article is Q-MRI applications of proton density and the 2 primary relaxation times (T1 and T2); however, most of these

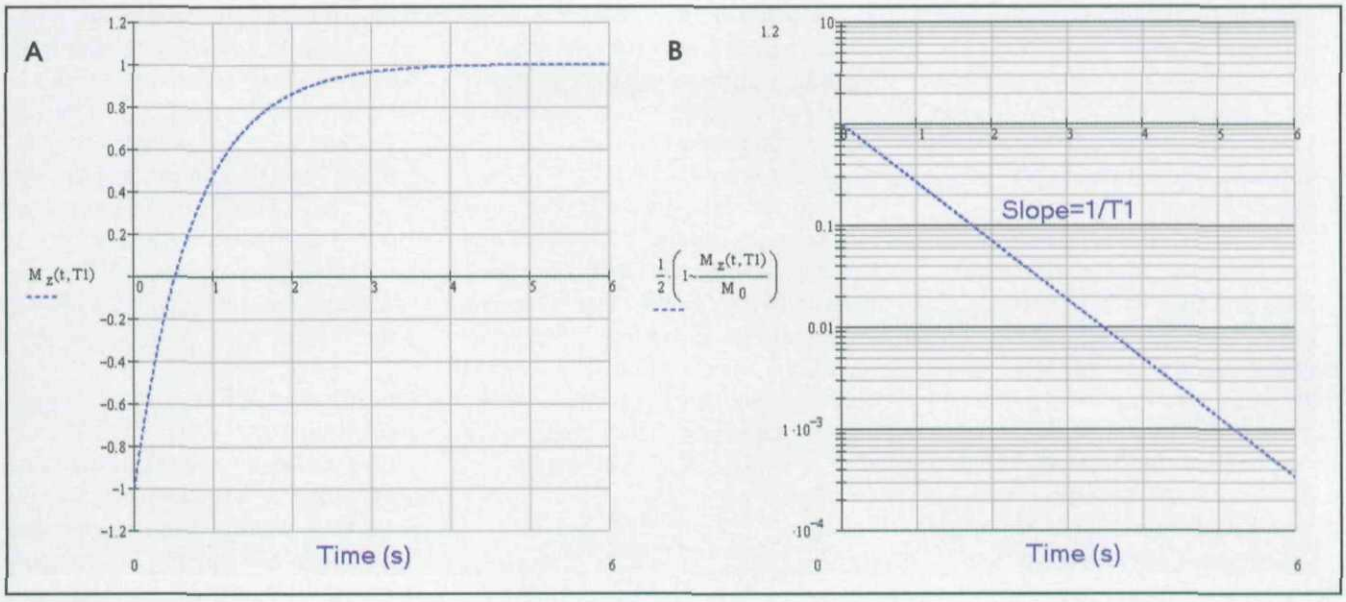

FIGURE 1. (A) Longitudinal relaxation time (T1) recovery curve and (B) semilogarithmic plot showing derivation of T1 relaxation time from the slope by varying inversion time (TI, in milliseconds).

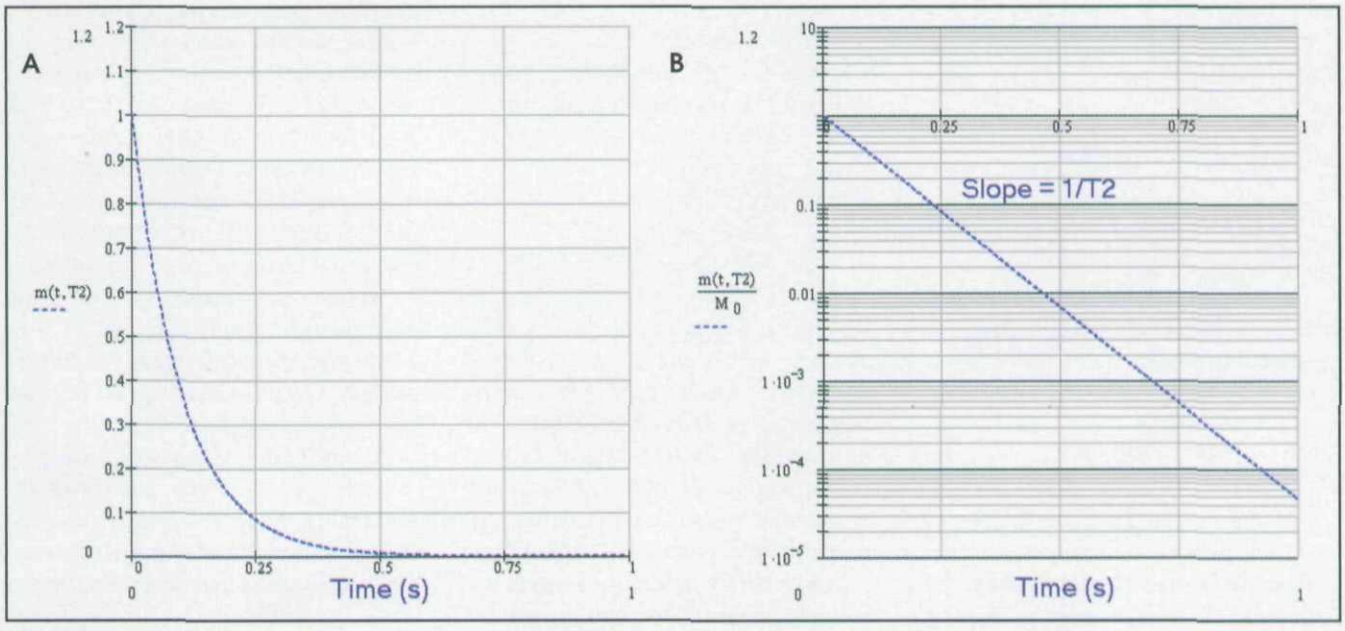

FIGURE 2. (A) Transverse relaxation time (T2) decay curve and (B) semilogarithmic plot showing derivation of T2 relaxation time from the slope by varying echo times (TE, in milliseconds).

principles and techniques apply to many other parameters such as diffusion, flow, magnetization transfer, and so forth. Although the principle of quantitative MRI by differential weighting applies to many tissue parameters, the pulse sequences and quantitative MRI post-processing algorithms are, in general, very different from tissue parameter to tissue parameter.

Origins of quantitative MR imaging

Using nuclear MR (NMR) relaxometry to detect disease predates the advent of MR imaging. Damadian[1] first reported alteration of T1 relaxation times in cancerous tumors in 1971. In the early 1980s, vast amounts of experimental quantitative NMR measurements of biological tissues (animal and human, normal and diseased) were published and reviewed by Bottomley and colleagues.[2,3] Crooks and coworkers[4] also speculated on the value of relaxation times in MR imaging.

Extrapolating to MR imaging this "NMR-relaxometry-disease-signature" concept was logical and intellectually appealing. Indeed, many seminal papers on Q-MRI pulse sequence design and theory were published in the early 1983 to 1988 period, only a few years after

the advent of clinical MR imaging.[5-15] Whereas quantitative NMR relaxometry applies to tissues on a whole-specimen basis, quantitative MR imaging is analogous to performing many quantitative NMR measurements in parallel on the much smaller voxel size scale.

T1 quantitative MR imaging

T1 is a measure of the promptness of a tissue to return to its longitudinal state of magnetic equilibrium, M_0, after removal from equilibrium with an RF pulse. This equilibration phenomenon is caused by interactions with the tissue lattice; hence, T1 is known as the spin-lattice relaxation time. The equilibration of the longitudinal magnetization is an exponential recovery process; for example, after application of a 180° inversion pulse in the setting of very long repetition times (TR), the longitudinal magnetization recovery as a function of time (Figure 1) can be approximated by the equation:

$$M_{Long}(t) = M_0\left(1 - 2\exp\left[-\frac{t}{T1}\right]\right)$$

Equation 1

This equation can be rearranged with basic algebraic manipulations to give the following:

$$\ln\left[\frac{1}{2}\left(1 - \frac{M_{Long}(t)}{M_0}\right)\right] = -\frac{t}{T1}$$

Equation 2

Hence, if the logarithmic quantity in the left-hand side is plotted as function of time, a straight line is predicted. Furthermore, the slope of this line is equal to the inverse of T1. This is the basis of Q-MRI algorithms for estimating T1 with multi-inversion time (TI) experiments. Theoretically, a minimum of only 2 points (ie, 2 inversion times) is required to determine the slope of this line, and, hence T1, though more measured points result in a more accurate slope estimation with noisy data. A comprehensive discussion of T1 calculations can be found in a recent review by Kingsley.[16]

T2 quantitative MR imaging

T2 is a measure of the promptness of a tissue to return to its null transverse state of magnetic equilibrium, after removal from equilibrium with a radiofrequency excitation pulse. This equilibration phenomenon is caused by interactions with other spins; accordingly, T2 is known as the spin-spin relaxation time. The equilibration of the transverse magnetization is an exponential decay process; for example, after application of a 90° excitation pulse, the transverse magnetization decay as a function of time in the setting of very long TRs (Figure 2) is approximated by the equation:

$$M_{Trans}(t) = M_0\ \exp\left[-\frac{t}{T2}\right]$$

Equation 3

As in the case of T1, this equation can be rearranged with basic algebraic manipulations resulting in the following:

$$\ln\left[\frac{M_{Tran}(t)}{M_0}\right] = -\frac{t}{T2}$$

Equation 4

Hence, if the logarithmic quantity in the left-hand side is plotted as function of time, a straight line is predicted. Furthermore, the slope of this line is equal to the inverse of T2. This is the basis of Q-MRI algorithms for estimating T2 with multi–spin-echo experiments. Again, a minimum of only 2 points (ie, 2 echo times) are required to determine the slope of this line, and hence T2, though more measured points result in a more accurate slope estimation with noisy data.

Proton density quantitative MR imaging

When TR is very long and TE (time to echo) is very short, the MR signal is directly proportional to the unweighted number of spinning protons present in the scanned volume. Images acquired with such a technique are minimally weighted by the relaxation times and are, therefore, termed PD weighted. Thus, the PD of each voxel forms the base image matrix upon which T1 weighting (by shortening TR) and T2 weighting (by prolonging TE) add contrast information. Proton density is proportional to, and according to Equation 1 or 3, can be quantified together with T1 or T2, respectively, as the extrapolated value of the transverse magnetization in the limit of infinitely short TE (ie, the y-axis intercepts in Figure 1B and 2B at a time of 0 msec).

Quantitative MR imaging pulse sequences

Many Q-MRI pulse sequences based on the differential weighting principle have been described in the literature. T2 differential weighting is commonly obtained via multi-echo imaging while partial saturation and inversion recovery (IR) have been used for T1 differential weighting. Some interrogate slices at many relaxation time points while some use the theoretical minimum of 2 time points. Almost all MR signal types have been used including gradient echoes, spin echoes, and hybrid readout methods (fast or turbo spin echo and echoplanar imaging).[16] Many of these Q-MRI pulse sequences target a single relaxation parameter, but a few are capable of targeting multiple parameters (T1, T2, and PD) in a single scan. Some described Q-MRI pulse sequences interrogate 1 slice per scan and others provide volume coverage.

As with MRI in general, increasing the scanning speed of Q-MRI is of paramount importance for clinical acceptance. The main roadblock to faster Q-MRI has been the loss of quantitative accuracy possibly associated with increasing imaging speed. Possible sources of error include imperfection of RF pulses in multislice imaging, interslice crosstalk, magnetization transfer effects, and computational inaccuracies from using a reduced number of time points with real data that, in general, contains varying levels of noise. The theoretical "gold standard" Q-MRI pulse sequences are fully relaxed (ie, infinite TR), are single-slice, and interrogate tissues at an infinite number of relaxation time points. To illustrate the slowness of such an approach, to generate one 256 × 256 T2 map with a

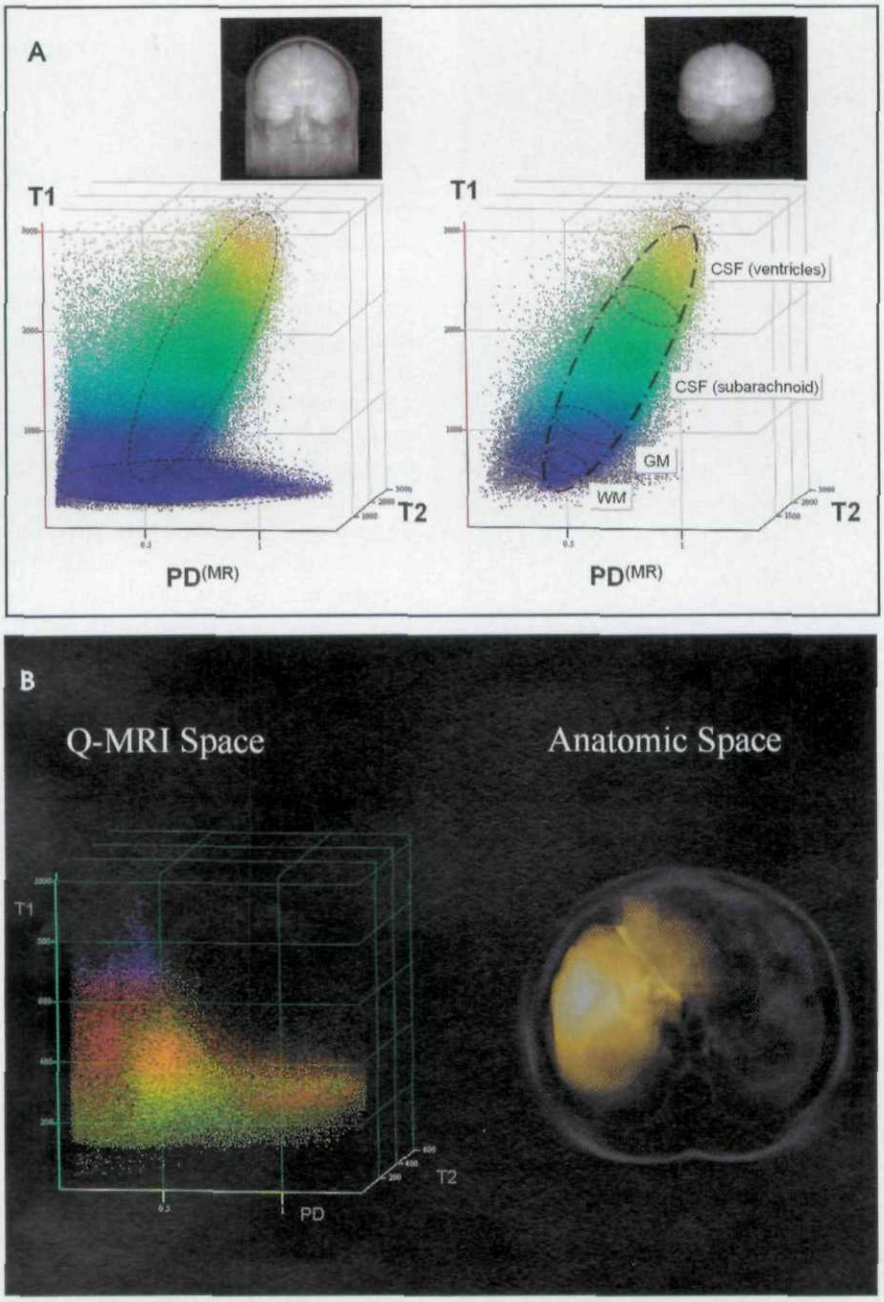

FIGURE 3. *(A) Perspective view of a 3-dimensional scatter plot of longitudinal relaxation time (T1, in milliseconds) versus transverse relaxation time (T2, in milliseconds) versus proton density (PD) (quantitative magnetic resonance imaging [Q-MRI] space) shows the distribution of voxels in this image of the brain organized by MR properties. The plot and rendered projection on the left illustrates all tissues in the scanned volume, whereas the plot and projection on the right only includes a segmented volume representing intracranial contents. Plots such as this may be used to segment voxels pertaining to a particular tissue type or organ (in this case, gray matter [GM], white matter [WM], and cerebrospinal fluid [CSF]). (B) Quantitative magnetic resonance imaging (Q-MRI) space formed with whole abdomen and segmented liver. Directly acquired images were generated with the mixed turbo spin-echo pulse sequence. The segmented liver is shown in anatomic space (right) and as a localized cluster in Q-MRI space (left). In anatomic space, the data are presented as an inferior-superior projection with the segmented liver superimposed onto a projection of the whole abdomen. In Q-MRI space, the cluster representing the liver (orange and yellow points) is superimposed onto the larger cluster representing all abdominal tissues (remaining points).*

multi–spin-echo sequence operating at 8-second TR, a scan time >34 minutes results.

Postprocessing options

Quantitative maps of T1, T2, and PD are not the only end products of Q-MRI. These data-rich maps may be further processed using a wide variety of approaches to yield information that may be more clinically useful. Computer postprocessing of Q-MRI data is a natural next step in data interpretation and may involve techniques such as segmentation, volumetry, structural analysis, and the generation of MR images with computer-synthesized T1 and T2 contrast weightings (Figures 6 and 7).

Q-MRI maps may be used as source data for semiautomated or automated segmentation into organs or tissue types based on MR biophysical properties.[17-24] Particular voxel subsets may be chosen from a multiaxis plot of values such as T1, T2, and PD (Figure 3). Voxel spatial relationships may also be combined with Q-MRI relationships to aid in anatomic segmentation (Figure 4). Segmentation serves as an intermediate step in quantification of organ volumes as well as in generation of frequency histograms. Frequency histograms may also be generated from the entire scan data set or segmented subsets of organs or tissue types (Figure 5).

Weighted combinations of co-registered Q-MRI maps may be used to create synthetic MR images that mimic directly acquired images (Figures 6 and 7).[7,8,25] Though these image sets may resemble their traditional MRI counterparts, they differ significantly in that the radiologist may vary the degree of T1, T2, PD, and IR weighting at the time of reading. The most tangible benefit to this type of imaging would be the enormous potential time savings possible in replacing multiple pulse sequences in a conventional MR examination with a single Q-MRI pulse sequence. Relative weighting may be varied analogous to windowing and leveling in a CT study.

Clinical applications of relaxometric quantitative MR imaging: A review

Q-MRI techniques that are becoming mainstream in current clinical practice

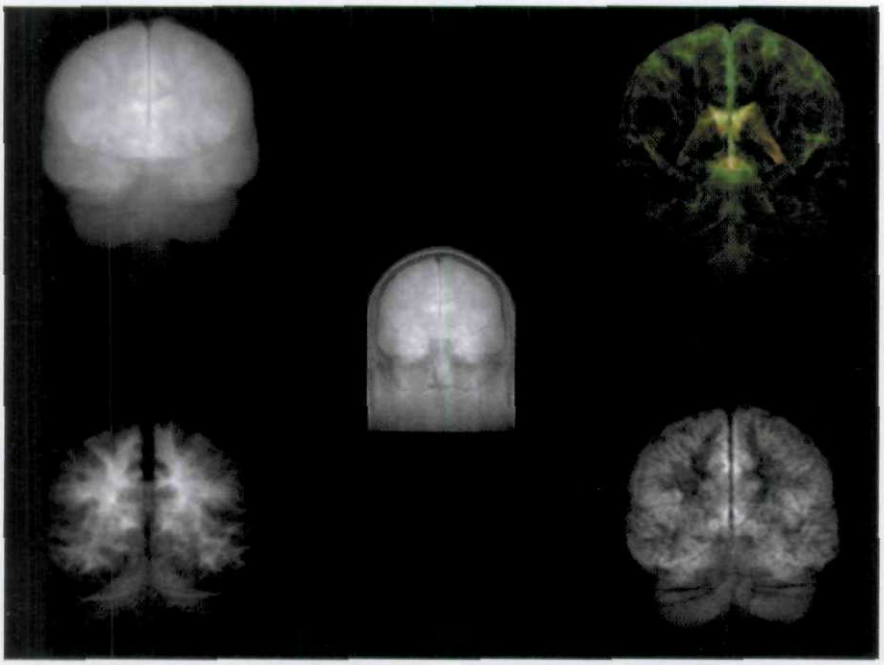

FIGURE 4. *Segmentation of tissue types in the brain. Projections of (clockwise from upper left): gray and white matter, cerebrospinal fluid, gray matter, and white matter. Center: whole head.*

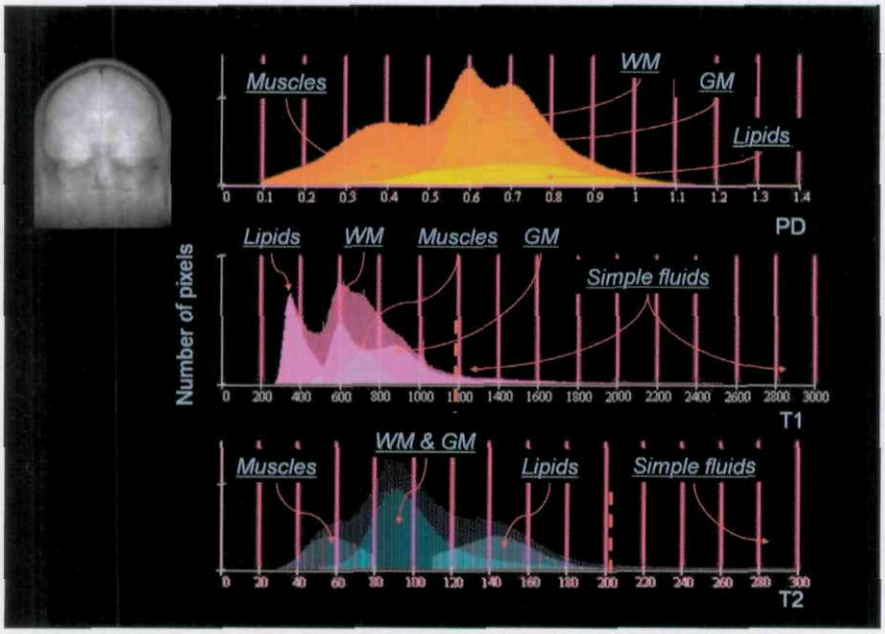

FIGURE 5. *Quantitative magnetic resonance distribution histograms of the brain. Frequency histograms of proton density (PD), longitudinal relaxation time (T1), and transverse relaxation time (T2) are plotted against relaxation time showing normal distributions for gray matter (GM), white matter (WM), cerebrospinal fluid, muscle, and lipids.*

include diffusion and perfusion in the setting of cerebral ischemia and infarction. Although these techniques are quantitative, in current clinical practice, the information is usually interpreted in a subjective manner using visual inspection of the maps to detect relative differences in pixel brightness (eg, apparent diffusion coefficient [ADC] and perfusion maps) in much the same way directly acquired images are interpreted.

Though applications of Q-MRI specific to quantification of T1, T2, and PD have been discussed in the scientific literature, they have not yet found routine use in clinical practice. A review of promising clinical applications follows.

Neurologic imaging

As with many early MRI techniques, one of Q-MRI's first demonstrations in humans was in the brain. As an examination that is less prone to motion artifact than imaging of other body parts, quantification of relaxation times in gray and white matter as well as cerebrospinal fluid was an attractive initial application for the Q-MRI technique. Almost all Q-MRI pulse sequences have been tested in the brain showing the normal Q-MRI brain architecture.[26-37] A complete review is outside the scope of this paper and can be found in the book edited by Tofts.[38] Pathological deviations studied with Q-MRI include the effects of iron deposition in patients with Parkinson's disease,[34,39] abnormal Q-MRI measures in multiple sclerosis plaques,[17,40-42] as well as cerebral edema related to stroke.[43,44] Q-MRI relaxometric studies of patients with schizophrenia[45] and with human immunodeficiency virus infection[46] have also been published.

Q-MRI brain postprocessing applications include generation of distribution histograms[38] as well as segmentation, quantification, and characterization of tissue types, such as gray matter, white matter, and cerebrospinal fluid.[17,41,44] These methods have also been applied to the human orbit with separation of extraocular muscles and retrobulbar fat from the globe.[47]

Synthetic MR images in the brain have been generated by multiple groups using Q-MRI acquisition techniques with close resemblance to directly acquired images.[7,8,25,48,49]

Abdominal imaging (liver, spleen)

Another application in clinical practice includes the characterization of liver lesions. T1 and T2 relaxation times measured by echoplanar methods have been shown to be helpful in the evaluation of focal lesions.[50] Dual-echo T2 techniques using traced regions of interest have also proved to be more accurate than conventional qualitative visual methods in differentiating benign from malignant foci.[51,52]

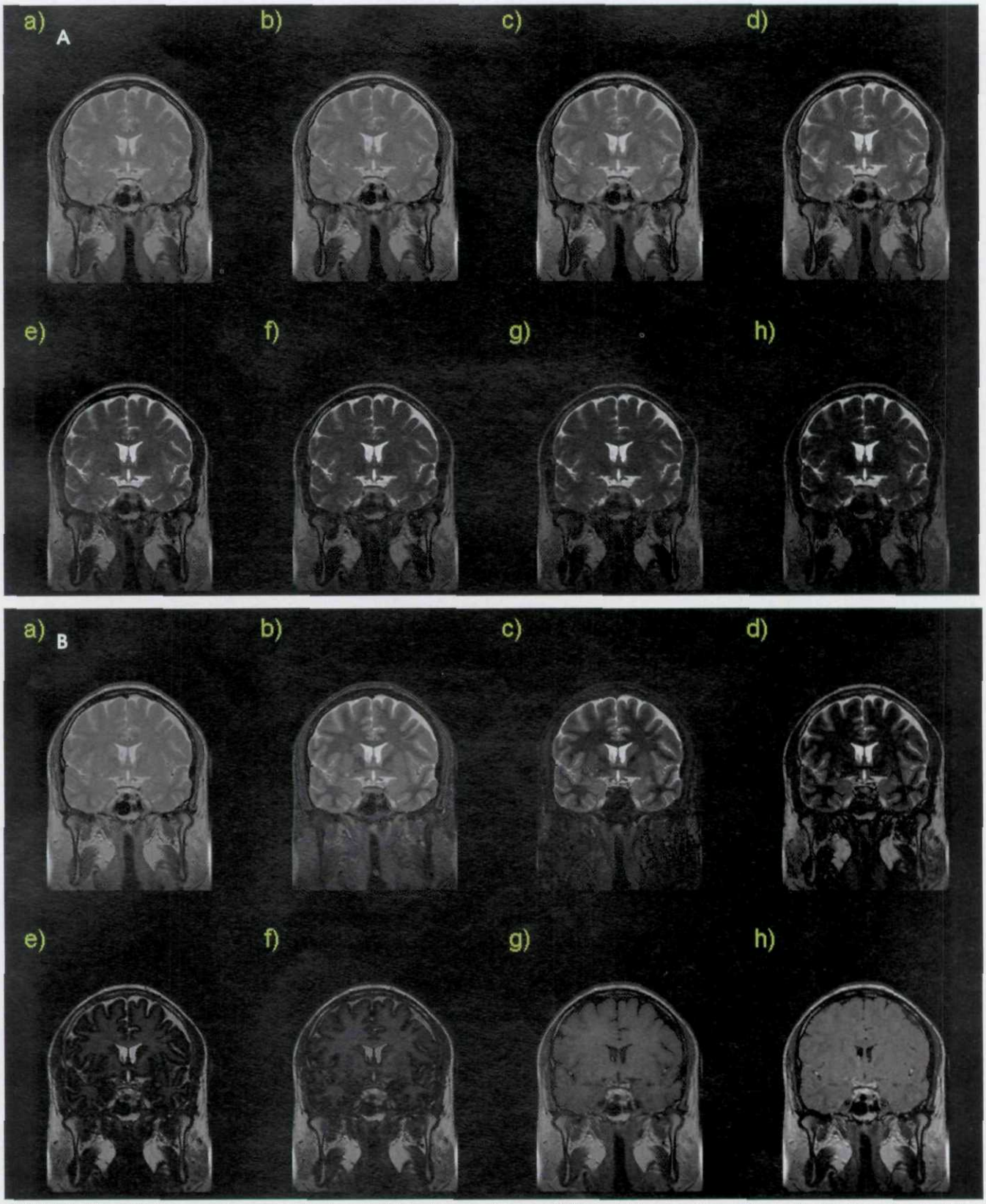

FIGURE 6. *Magnetic resonance image synthesis in the brain. Images of user variable weighting may be synthesized at the time of image interpretation. (A) User-varied echo times (TE, in milliseconds) and constant long TR. a) TE = 0, b) TE = 10, c) TE = 15, d) TE = 30, e) TE = 60, f) TE = 90, g) TE = 120, h) TE = 200. (B) User-varied inversion times (TI, in milliseconds). a) TI = 0, b) TI = 150, c) TI = 300, d) TI = 450, e) TI = 600, f) TI = 750, g) TI = 1500, h) TI = 2500.*

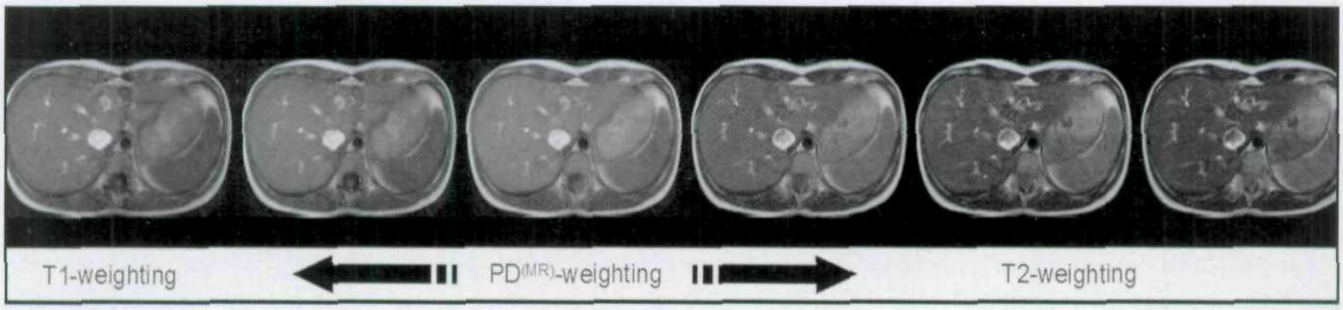

FIGURE 7. *Magnetic resonance image synthesis in the abdomen. Images of user-variable weighting may be synthesized at the time of image interpretation. PD = proton density.*

These techniques have not found widespread use, however, perhaps due to the perceived complexity of relaxation time calculation.

The amount of hepatic iron deposition in diseases such as primary and secondary hemochromatosis has been repeatedly shown to correlate closely with T2 and T2* relaxivity.[53-55] Q-MRI may be used not only to determine the severity of iron deposition, but also to monitor response to medical therapy.[56] Other diffuse liver diseases that may benefit from Q-MRI analysis include steatosis, hepatitis, and cirrhosis; however, further work is needed to determine Q-MRI efficacy in these disease processes.

As in the brain and orbit, synthetic MR images of the liver and spleen have also been generated with the same capacity for the radiologist to vary T1, T2, and IR weighting at the time of image interpretation.[19,22]

Pelvis (prostate, uterus)

Q-MRI has been applied to both the male and female pelvis for both prostate and uterine imaging. Fast Q-MRI imaging of the prostate has met with some success, especially in the measurement of water content and its correlation with citrate concentration in predicting prostate cancer.[57] Q-MRI techniques have also been used recently to measure T1 and T2 relaxation times of the normal female uterus at 1.5T and 3.0T.[58]

Thorax (lung, heart, and breast)

Lung T1 relaxation times and changes in T1 with oxygenation have been shown by using snapshot fast low-angle shot (FLASH), a gradient-echo pulse sequence.[59] At least one study of lung T2 relaxation time has been performed ex vivo in juvenile pigs.[60]

Most quantitative work being performed in the thorax, however, has concentrated on the myocardium. T2 maps have been generated in vivo (human) and T2* maps ex vivo (beating rat hearts) in attempts to correlate T2 and T2* prolongation to decreased oxygen microcirculation and ischemia with good result.[61,62] T1 relaxation times of myocardium have also been measured and mapped in healthy hearts as well as in myocardial infarction.[63]

Quantitative approaches to contrast kinetics have also been described by multiple groups for use in evaluating myocardial enhancement as well as contrast enhancement in breast imaging. TurboFLASH and T1 fast-acquisition relaxation mapping (T1 FARM) pulse sequences have been used to successfully quantify myocardial perfusion via measured changes in T1 relaxivity.[64,65] The FLASH pulse sequence has also been used to acquire T1 maps of the breast before and after contrast administration to calculate a concentration-time curve and potentially improve breast MR diagnostic accuracy.[66]

Fetal/pediatric (brain development, lung maturity, placenta)

Q-MRI techniques have also found uses in fetal and pediatric MR imaging of developing organs. Much of the early neuroradiologic Q-MRI research focused on myelin characterization of the developing fetal and pediatric brain through measurements of T1 relaxation time in white matter showing a clear relationship between the time course of T1 relaxivity changes with age.[35,67,68] T1 relaxation times were also shown to be significantly different from controls in children with sickle cell disease (significantly higher before the age of 2 years and significantly lower by the age of 4 years).[69,70]

Both T1 and T2 measurements have been made in vivo in the preterm human placenta showing significant decrease in T1 relaxation times in placentas of compromised pregnancies (pre-eclampsia and intrauterine growth restriction) compared with times in those of controls. This has been postulated to be due to placental infarction and fibrosis.[71] A similar in vivo assay has been applied to measurements of fetal lung maturity, showing a relationship of both T1 and T2 to gestational age and lung volume.[72] The implications for these studies include potential noninvasive quantitative approaches to measuring fetal health.

Musculoskeletal (bone marrow, cartilage)

Various Q-MRI approaches have been used to characterize marrow lipid and trabecular bone in the human skeleton. Estimates of marrow lipid content have been made with line scan spin-echo techniques (both conventional and fast spin echo).[73] Gradient-echo sequences have also been applied to marrow lipid to measure T2*.[74] These T2* measures correlated well with dual energy X-ray absorptiometry bone mineral density measurements, indicating that marrow T2* relaxation may be correlated to trabecular bone content. Distribution histograms have also been generated from T1 and T2 measures of bone.[75]

Ex vivo and in vivo measures of T1 and T2 for skeletal muscle were attempted

using both NMR spectroscopy as well as MRI as early as 1986.[76] In a later experiment, in vivo T2 measures were shown with multicomponent T2 histograms of at least 4 differing populations of protons in the flexor digitorum profundus.[77]

Applications in cartilage have included spin-echo measures of T2 in human cartilage.[78] T2 times increase with early osteoarthritis and then decrease with more severe osteoarthritis. T2 maps have also shown significant intercompartment and intracompartment variability, reflecting focal cartilage defects seen in early osteoarthritis.

Conclusion

While the concept of using magnetic resonance as a quantitative tool predates the development of MR imaging, the clinical practice of MR imaging has been predominantly qualitative for much of its history. With the ongoing development of more powerful and precise scanner and computer hardware, as well as innovations in fast pulse sequence design, Q-MRI is rapidly becoming clinically feasible. T1 and T2 relaxation times and PD may be measured and mapped with a variety of pulse sequences, including ones that measure all 3 properties simultaneously. Use of coregistered maps of T1, T2, and PD may be further postprocessed for segmentation and volumetry, generation of distribution histograms, as well as derivation of synthetic MR images. An exciting potential future ap-plication utilizing Q-MRI postprocessing may even include design of computer-aided detection/diagnosis tools. Q-MRI techniques have already been shown in many organ systems throughout the human body in an effort to improve diagnostic sensitivity as well as monitor therapy. As these methods employ conventional MR scanning equipment, Q-MRI shows the potential for widespread adoption in clinical practice as well as the promise of more automated and efficient MR image processing.

References

1. Damadian R. Tumor detection by nuclear magnetic resonance. *Science.* 1971;171:1151-1153.
2. Bottomley PA, Foster TH, Argersinger RE, Pfeifer LM. A review of normal tissue hydrogen NMR relaxation times and relaxation mechanisms from 1-100 MHz: Dependence on tissue type, NMR frequency, temperature, species, excision, and age. *Med Phys.* 1984;11:425-448.
3. Bottomley PA, Hardy CJ, Argersinger RE, Allen-Moore G. A review of 1H nuclear magnetic resonance relaxation in pathology: Are T1 and T2 diagnostic? *Med Phys.* 1987;14:1-37.
4. Crooks LE, Hylton NM, Ortendahl DA, et al. The value of relaxation times and density measurements in clinical MRI. *Invest Radiol.* 1987;22:158-169.
5. Schneiders NJ, Post H, Brunner P, et al. Accurate T2 NMR images. *Med Phys.* 1983;10:642-645.
6. Parker DL, Smith V, Sheldon P, et al. Temperature distribution measurements in two-dimensional NMR imaging. *Med Phys.* 1983;10:321-325.
7. Ortendahl DA, Hylton NM, Kaufman L, Crooks LE. Signal to noise in derived NMR images. *Magn Reson Med.* 1984;1:316-338.
8. Riederer SJ, Suddarth SA, Bobman SA, et al. Automated MR image synthesis: Feasibility studies. *Radiology.* 1984;153:203-206.
9. Schneiders NJ, Ford JJ, Bryan RN. Accurate T1 and spin density NMR images. *Med Phys.* 1985;12:71-76.
10. Graumann R, Fischer H, Oppelt A. A new pulse sequence for determining T1 and T2 simultaneously. *Med Phys.* 1986;13:644-647.
11. O'Donnell M, Gore JC, Adams WJ. Toward an automated analysis system for nuclear magnetic resonance imaging: I. Efficient pulse sequences for simultaneous T1-T2 imaging. *Med Phys.* 1986;13:182-190.
12. MacFall JR, Riederer SJ, Wang HZ. An analysis of noise propagation in computed T2, pseudodensity, and synthetic spin-echo images. *Med Phys.* 1986;13:285-292.
13. Lee JN, Riederer SJ, Bobman SA, et al. The precision of TR extrapolation in magnetic resonance image synthesis. *Med Phys.* 1986;13:170-176.
14. In den Kleef JJ, Cuppen JJ. RLSQ: T1, T2, and rho calculations, combining ratios and least squares. *Magn Reson Med.* 1987;5:513-524.
15. Hinson WH, Sobol WT. A new method of computing spin-lattice relaxation maps in magnetic resonance imaging using fast scanning protocols. *Med Phys.* 1988;15:551-561.
16. Kingsley PB. Methods of measuring spin-lattice (T1) relaxation times: An annotated bibliography. *Concepts Magn Reson.* 1999;11:243-276.
17. Alfano B, Brunetti A, Larobina M, et al. Automated segmentation and measurement of global white matter lesion volume in patients with multiple sclerosis. *J Magn Reson Imaging.* 2000;12:799-807.
18. McGinnis P, Jensen M, Barest G, et al. Initial experience with virtual magnetic resonance imaging of the human brain: A comparison of quantitative-based synthetic magnetic resonance imaging to a standard clinical protocol. Presented at the 49th Annual Meeting of the Association of University Radiologists, Toronto, Canada, May 2001.
19. Jara H, Soto JA. Physical principles and potential applications of MR scanning with the mixed turbo spin-echo pulse sequence [abstract]. *Radiology.* 2002; 225(P):715.
20. Hartman E, Soto JA, McKinstry EL, Jara H. Automated liver segmentation and volumetric quantification: A new application of the mixed turbo spin echo pulse sequence. Presented at the 88th Scientific Assembly and Annual Meeting of the Radiological Society of North America, Chicago, IL, December 2002.
21. McKinstry EL, Jara H. Volumetry of the human brain: A novel segmentation algorithm combining structural quantitative MRI with voxel connectivity. Presented at the 11th Scientific Meeting and Exhibition of the International Society for Magnetic Resonance in Medicine, Toronto, Canada, July 2003.
22. Farraher SW, Chang KJ, McKinstry EL, et al. Liver and spleen volume measurements: Comparison of a semi-automated quantitative MRI (Q-MRI) segmentation technique vs. segmentation with manual tracing. Presented at the 89th Scientific Assembly and Annual Meeting of the Radiological Society of North America, Chicago, IL, December 2003.
23. McKinstry EL, Chang KJ, Farraher SW, et al. Quantitative magnetic resonance imaging (Q-MRI) spectroscopy (PD, T1, and T2) of the liver and spleen: Whole organ characterization in 20 patients. Presented at the 89th Scientific Assembly and Annual Meeting of the Radiological Society of North America, Chicago, IL, December 2003.
24. Farraher SW, Chang K, McKinstry EL, et al. Applications of the mixed TSE sequence in the abdomen: Semi-automated volumetry, virtual MRI, and whole organ Q-MRI spectral analysis. Presented at the 89th Scientific Assembly and Annual Meeting of the Radiological Society of North America, Chicago, IL, December 2003.
25. Jara, H. Synthetic images for a magnetic resonance imaging scanner using linear combination of source images to generate contrast and spatial navigation. United States patent serial number: 09/779, 770 (2004).
26. Cho S, Jones D, Reddick WE, et al. Establishing norms for age-related changes in proton TI of human brain tissue in vivo. *Magn Reson Imaging.* 1997;15: 1133-1143.
27. Whittall KP, MacKay A, Graeb DA, et al. In vivo measurement of T2 distributions and water contents in normal human brain. *Magn Reson Med.* 1997;37:34-43.
28. Wansapura JP, Holland SK, Dunn RS, Ball WS. NMR relaxation times in the human brain at 3.0 Tesla. *J Magn Reson Imaging.* 1999;9:531-538.
29. Henderson E, McKinnon G, Lee TY, Rutt BK. A fast 3D Look-Locker method for volumetric T1 mapping. *Magn Reson Imaging.* 1999;17:1163-1171.
30. Karlsson M, Nordell B. Phantom and in vivo study of the Look-Locher T1 mapping method. *Magn Reson Imaging.* 1999;17:1481-1488.
31. Imran J, Langevin F, Saint-Jalmes H. Two-point method for T1 estimation with optimized gradient-echo sequence. *Magn Reson Imaging.* 1999;17:1347-1356.
32. McKenzie CA, Chen Z, Drost DJ, Prato FS. Fast acquisition of quantitative T2 maps. *Magn Reson Med. 1999;41:208-212.*
33. Deichmann R, Hahn D, Haase A. Fast T1 mapping on a whole-body scanner. *Magn Reson Imaging.* 1999;42:206-209.
34. Vymazal J, Righini A, Brooks RA, et al. T1 and T2 in the brain of healthy subjects, patients with Parkinson disease, and patients with multiple system atrophy: Relation to iron content. *Radiology.* 1999;211:489-495.
35. Haselgrove J, Moore J, Wang Z, et al. A method for fast multislice T1 measurement: Feasibility studies on phantoms, young children, and children with Canavan's disease. *J Magn Reson Imaging.* 2000;11:360-367.
36. Steinhoff S, Zaitsev M, Zilles K, Shah NJ. Fast T1 mapping with volume coverage. *Magn Reson Imaging.* 2001;46:131-140.
37. Deoni SC, Rutt BK, Peters TM. Rapid combined T1 and T2 mapping using gradient recalled acquisition in the steady state. *Magn Reson Med.* 2003;49:515-526.
38. Tofts P, ed. *Quantitative MRI of the Brain: Measuring Changes Caused by Disease.* Hoboken, NJ: John Wiley & Sons; 2005.
39. Bartzokis G, Cummings JL, Markham CH, et al. MRI evaluation of brain iron in earlier- and later-onset

Parkinson's disease and normal subjects. *Magn Reson Imaging.* 1999;17:213-222.
40. Srinivasan R, Henry R, Pelletier, D, Nelson S. Standardized, reproducible, high resolution global measurements of T1 relaxation metrics in cases of multiple sclerosis. *AJNR Am J Neuroradiol.* 2003;24:58-67.
41. Parry A, Clare S, Jenkinson M, et al. MRI brain T1 relaxation time changes in MS patients increase over time in both the white matter and the cortex. *J Neuroimaging.* 2003;13:234-239.
42. Whittall KP, MacKay AL, Li DK, et al. Normal-appearing white matter in multiple sclerosis has heterogeneous, diffusely prolonged T2. *Magn Reson Med.* 2002;47:403-408.
43. Fatouros PP, Marmarou A, Kraft KA, et al. In vivo brain water determination by T1 measurements: Effect of total water content, hydration fraction, and field strength. *Magn Reson Med.* 1991;17:402-413.
44. Bernarding J, Braun J, Hohmann J, et al. Histogram-based characterization of healthy and ischemic brain tissues using multiparametric MR imaging including apparent diffusion coefficient maps and relaxometry. *Magn Reson Med.* 2000;43:52-61.
45. Supprian T, Hofmann E, Warmuth-Metz M, et al. MRI T2 relaxation times of brain regions in schizophrenic patients and control subjects. *Psychiatry Res.* 1997;75:173-182.
46. Miszkiel KA, Paley MN, Wilkinson ID, et al. The measurement of R2, R2*, and R2' in HIV-infected patients using the prime sequence as a measure of brain iron deposition. *Magn Reson Imaging.* 1997;15:1113-1119.
47. Jara H, Fleming K, Sakai O. PD, T1, and T2 quantitative MRI spectroscopy of the orbit: An application of the Mix-TSE pulse sequence. Presented at the 12th Scientific Meeting and Exhibition of the International Society for Magnetic Resonance in Medicine, Kyoto, Japan, May 2004.
48. Schmitt P, Griswold MA, Jakob PM, et al. Inversion recovery TrueFISP: Quantification of T1, T2, and spin density. *Magn Reson Med.* 2004;51:661-667.
49. Gulani V, Schmitt P, Griswold MA, et al. Multiple contrast mechanisms in synthetic images calculated from a single IR TrueFISP experiment. Presented at the 12th Scientific Meeting and Exhibition of the International Society for Magnetic Resonance in Medicine, Kyoto, Japan, May 2004.
50. Goldberg MA, Hahn PF, Saini S, et al. Value of T1 and T2 relaxation times from Echoplanar MR imaging in the characterization of focal hepatic lesions. *AJR Am J Roentgenol.* 1993;160:1011-1017.
51. Fenlon HM, Tello R, deCarvalho VL, Yucel EK. Signal characteristics of focal liver lesions on double echo T2-weighted conventional spin echo MRI: Observer performance versus quantitative measurements of T2 relaxation times. *J Comput Assist Tomogr.* 2000;24: 204-211.
52. Tello R, Fenlon HM, Gagliano T, et al. Prediction rule for characterization of hepatic lesions revealed on MR imaging: Estimation of malignancy. *AJR Am J Roentgenol.* 2001;176:879-884.
53. Clark PR, St. Pierre TG. Quantitative mapping of transverse relaxivity (1/T2) in hepatic iron overload: A single spin-echo imaging methodology. *Magn Reson Imaging.* 2000;18:431-438.
54. Papakonstantinou OG, Maris TG, Kostaridou V, et al. Assessment of liver iron overload by T2-quantitative magnetic resonance imaging: Correlation of T2-QMRI measurements with serum ferritin concentration and histologic grading of siderosis. *Magn Reson Imaging.* 1995;13:967-977.
55. Deoni SC, Kost JA, Adams PA, et al. Quantification of liver iron with rapid 3D R1 and R2 mapping with DESPOT1 and DESPOT2. Presented at the 12th Scientific Meeting and Exhibition of the International Society for Magnetic Resonance in Medicine, Kyoto, Japan, May 2004.
56. Clark P, Chua-anusorn W, St. Pierre T. Liver iron measurement and mapping using MRI. Presented at the 12th Scientific Meeting and Exhibition of the International Society for Magnetic Resonance in Medicine, Kyoto, Japan, May 2004.
57. Liney GP, Knowles AJ, Manton DJ, et al. Comparison of conventional single echo and multi-echo sequences with a fast spin-echo sequence for quantitative T2 mapping: Application to the prostate. *J Magn Reson Imaging.* 1996;6:603-607.
58. de Bazelaire CM, Duhamel GD, Rofsky NM, Alsop DC. MR imaging relaxation times of abdominal and pelvic tissues measured in vivo at 3.0T: Preliminary results. *Radiology.* 2004;230:652-659.
59. Jakob PM, Hillenbrand CM, Wang T, et al. Rapid quantitative lung 1H T1 mapping. *J Magn Reson Imaging.* 2001;14:795-799.
60. Estilaei M, MacKay A, Whittall KP, Mayo J. In vitro measurements of water content and T2 relaxation times in lung using a clinical MRI scanner. *J Magn Reson Imaging.* 1999;9:699-703.
61. Foltz WD, Al-Kwifi O, Sussman MS, et al. Optimized spiral imaging for measurement of myocardial T2 relaxation. *Magn Reson Med.* 2003;49:1089-1097.
62. Köhler S, Hiller KH, Waller C, et al. Visualization of myocardial microstructure using high resolution T2* imaging at high magnetic field. *Magn Reson Med.* 2003;49:371-375.
63. Messroghli DR, Radjenovic A, Kozerke S, et al. Modified Look-Locker inversion recovery (MOLLI) for high-resolution T1 mapping of the heart. *Magn Reson Med.* 2004;52:141-146.
64. McKenzie CA, Pereira RS, Prato FS, et al. Improved contrast agent bolus tracking using T1 FARM. *Magn Reson Med.* 1999;41:429-435.
65. Bellamy DD, Pereira RS, McKenzie CA, et al. Gd-DTPA bolus tracking in the myocardium using T1 fast acquisition relaxation mapping (T1 FARM). *Magn Reson Med.* 2001;46:555-564.
66. Brookes JA, Redpath TW, Gilbert FJ, et al. Measurement of spin-lattice relaxation times with FLASH for dynamic MRI of the breast. *Br J Radiol.* 1996;69: 206-214.
67. Cho S, Jones D, Reddick WE, et al. Establishing norms for age-related changes in proton Tl of human brain tissue in vivo. *Magn Reson Imaging.* 1997;15: 1133-l 143.
68. Almajeed AA, Adamsbaum C, Langevin F. Myelin characterization of fetal brain with mono-point estimated T1-maps. *Magn Reson Imaging.* 2004;22:565-557.
69. Steen RG, Reddick WE, Mulhern R, et al. Quantitative MRI of the brain in children with sickle cell disease reveals abnormalities unseen by conventional MRI. *J Magn Reson Imaging.* 1998;8:535-543.
70. Steen RG, Hunte M, Traipe E, et al. Brain T1 in young children with sickle cell disease: Evidence of early abnormalities in brain development. *Magn Reson Imaging.* 2004;22:299-306.
71. Gowland PA, Freeman A, Issa B, et al. In vivo relaxation time measurements in the human placenta using echo planar imaging at 0.5T. *Magn Reson Imaging.* 1998;16:241-247.
72. Duncan KR, Gowland PA, Freeman A, et al. The changes in magnetic resonance properties of the fetal lungs: A first result and a potential tool for the non-invasive in utero demonstration of fetal lung maturation. *Br J Obstet Gynaecol.* 1999;106:122-125.
73. Mulkern RV, Meng J, Bowers JL, et al. In vivo bone marrow lipid characterization with line scan Carr-Purcell-Meiboom-Gill proton spectroscopic imaging. *Magn Reson Imaging.* 1997;15:823-837.
74. Fransson A, Grampp S, Imhof H. Effects of trabecular bone on marrow relaxation in the tibia. *Magn Reson Imaging.* 1999;17:69-82.
75. Fantazzini P, Garavaglia C, Guglielmi G. Continuous distribution analysis of marrow 1H magnetic resonance relaxation in bone. *Magn Reson Imaging.* 2001;19:227-231.
76. LeBlanc A, Evans H, Schonfeld E, et al. Relaxation times of normal and atrophied muscle. *Med Phys.* 1986;13:514-517.
77. Saab G, Thompson RT, Marsh GD. Multicomponent T2 relaxation of in vivo skeletal muscle. *Magn Reson Med.* 1999;42:150-157.
78. David-Vaudey E, Ghosh S, Ries M, Majumdar S. T2 relaxation time measurements in osteoarthritis. *Magn Reson Imaging.* 2004;22:673-682.

THE AUTHORS

Kevin J. Chang, MD

Dr. Chang is currently a fourth-year Radiology Resident at Boston University Medical Center, Boston, MA. He earned his BA in Biology from the University of Pennsylvania, his BS in Health Care Management from the Wharton Undergraduate School of Business, and his MD from the University of Pennsylvania School of Medicine, Philadelphia, PA. He completed a transitional-year Internship at Advocate Ravenswood Medical Center, Chicago, IL, before entering residency. Dr. Chang will begin a Cross-Sectional Imaging Fellowship at Johns Hopkins Hospital, Baltimore, MD in 2005.

Hernán Jara, PhD

Dr. Jara is an Associate Professor of Radiology and an Adjunct Associate Professor in the School of Biomedical Engineering at the Boston University School of Medicine, Boston, MA.